Mineralium Deposita (2021) 56:991–1006
https://doi.org/10.1007/s00126-020-01025-0

ARTICLE

Sulfur isotopic compositions of sulfides along the Southwest Indian Ridge: implications for mineralization in ultramafic rocks

Teng Ding[1,2,3] · Chunhui Tao[1,3,4] · Ágata Alveirinho Dias[5,6] · Jin Liang[1] · Jie Chen[1] · Bin Wu[7] · Dongsheng Ma[8] · Rongqing Zhang[8] · Jia Wang[3] · Shili Liao[1] · Yuan Wang[1] · Weifang Yang[1] · Jia Liu[1] · Wei Li[1] · Guoyin Zhang[1] · Hui Huang[7]

Received: 28 April 2020 / Accepted: 22 October 2020 / Published online: 31 October 2020

Abstract

The recently explored Tianzuo hydrothermal field in serpentinized ultramafic rocks of the amagmatic segment of the ultraslow-spreading Southwest Indian Ridge displays high-temperature sulfide mineralization (isocubanite, sphalerite, and minor pyrrhotite) and low-temperature (pyrite and covellite) phases. Pyrite can be subdivided into pyrite-I and -II, with the former generally having a pseudomorphic texture after pyrrhotite and the latter typically growing around isocubanite, sphalerite, and pyrite-I or occurring as individual grains in quartz veinlets. The sulfide minerals have the greatest range of $\delta^{34}S$ values (− 23.8 to 14.1‰), found so far among modern sediment-starved ridges, with distinct $\delta^{34}S$ values for low- and high-temperature mineral phases. The high $\delta^{34}S$ values of isocubanite (9.6 to 12.2‰) and sphalerite (9.1 to 14.1‰) suggest that sulfate, which precipitated from seawater during an early low-temperature phase of hydrothermal circulation, was the main sulfur source for these sulfides. Pyrite-II has the lowest and most variable $\delta^{34}S$ values (− 23.8 to − 3.6‰), suggesting microbial sulfate reduction. Pyrite-I has variable and generally positive $\delta^{34}S$ values (− 0.1 to 12.0‰), with sulfur being inherited from pyrrhotite from the original thermochemical reduction of sulfate, mixed with volcanogenic sulfur. Intermittent magmatism represented by gabbroic intrusions, and high permeability caused by well-developed fractures associated with detachment faults, contributed to the formation of sulfides in the Tianzuo hydrothermal field. These factors possibly control sulfide mineralization in amagmatic segments of ultraslow-spreading ridges.

Keywords Tianzuo hydrothermal field · SWIR (Southwest Indian Ridge) · Ultramafic rocks · Sulfides · Sulfur isotopes

Editorial handling: M. Fiorentini

Supplementary Information The online version contains supplementary material available at https://doi.org/10.1007/s00126-020-01025-0.

✉ Chunhui Tao
taochunhuimail@163.com

[1] Key Laboratory of Submarine Geosciences, Second Institute of Oceanography, Ministry of Natural Resources, Hangzhou 310012, China

[2] Key Laboratory of Metallogenic Prediction of Nonferrous Metals and Geological Environment Monitoring, Central South University, Ministry of Education, Changsha 410083, China

[3] Institute of Marine Geology, College of Oceanography, Hohai University, Nanjing 210098, China

[4] School of Oceanography, Shanghai Jiaotong University, Shanghai 200030, China

[5] Institute of Science and Environment, University of Saint Joseph, Rua de Londres 106, Macao, China

[6] Instituto Dom Luiz, Faculty of Sciences of the University of Lisbon, Campo Grande, Ed. C1, Piso 1, Lisbon, Portugal

[7] State Key Laboratory of Nuclear Resources and Environment, East China University of Technology, Nanchang 330013, China

[8] State Key Laboratory for Mineral Deposits Research, Nanjing University, Nanjing 210046, China

Introduction

Spreading rates of oceanic ridges are commonly considered as superfast (> 140 mm yr^{-1}), fast (80–140 mm yr^{-1}), intermediate (55–80 mm yr^{-1}), slow (20–55 mm yr^{-1}), or ultraslow (< 20 mm yr^{-1}) (Dick et al. 2003 and references therein; Beaulieu et al. 2013). Since longitudinal profiles of ridges are closely associated with the intensity of magmatism (Standish and Sims 2010), and hydrothermal activity is significantly correlated with spreading rate (Baker et al. 1996; Baker 2009), previous studies considered that hydrothermal fields in oceanic ridges are predominantly controlled by the eruption and/or intrusion of basaltic magmas (Hannington et al. 2005; Fouquet et al. 2010). This results in most sulfide deposits being hosted in basalts, especially at fast-spreading ridges, with few being hosted in ultramafic rocks. However, in fast-spreading ridges, hydrothermal circulation may be blocked by such eruptions, resulting in abundant small-scale sulfide deposits (Fornari et al. 1998). Contrarily, sulfide deposits and vent sites in slow-spreading ridges tend to be much larger than those found in classic magmatic settings (German et al. 2016); in most cases, they are hosted in long-lived detachment faults (leading to oceanic core complex formation with exhumation of ultramafic rocks). This allows the formation of relatively stable and long-lived fluid pathways, and also the involvement of serpentinization reactions within the hydrothermal circulation cells (Hannington et al. 2005; McCaig et al. 2007; Ildefonse et al. 2007; Escartin et al. 2008; Fouquet et al. 2010).

Hydrothermal activity in slow-spreading ridges may be extensive (German and Parson 1998; Münch et al. 2001; Baker et al. 2004; Nayak et al. 2014), even in ultraslow ridges, where it was considered to be absent because of scarce magmatic activity (Baker et al. 1996). Tao et al. (2012) found an active black smoker chimney (Longqi field; 37.8° S, 49.6° E) in the ultraslow-spreading Southwest Indian Ridge (SWIR), showing that sulfide deposits develop in such environments, with hydrothermal activity being associated with localized magmatic activity and stable permeability. More hydrothermal fields have since been discovered near Longqi, including the Yuhuang (49.3° E), Xilongjing (49.7° E), Duanqiao (50.4° E), Changbai (~ 51.0° E), and Zhanqiao (~ 51.0° E) fields (Tao et al. 2014; Yang et al. 2017b; Liao et al. 2018). An important feature of ultraslow-spreading ridges is that they can be considered in terms of magmatic and amagmatic segments (Sauter et al. 2009; Standish and Sims 2010; Li et al. 2015; Yang et al. 2017a). The extensive occurrence of basalts suggests that SWIR fields, including the previously discovered inactive Mt. Jourdanne field at 63° 56′ E, are most likely associated with magmatic activity (Münch et al. 2001; Nayak et al. 2014; Tao et al. 2014; Yang et al. 2017b; Liao et al. 2018; Yuan et al. 2018).

Sulfide deposits associated with ultramafic rocks along the slow-spreading Mid-Atlantic Ridge (MAR) appear to be more abundant than in ophiolites on land (Fouquet et al. 2010), with ultramafic-hosted volcanogenic sulfide deposits being a specific marine mineralization type occurring along the MAR in the Logatchev (Bogdanov et al. 1997), Rainbow (German et al. 1996; Lein et al. 2001), Lost City (Kelley et al. 2001), Ashadze (Cherkashev et al. 2013), Menez Hom (Fouquet et al. 2002), Nibelungen (Melchert et al. 2008), Saldanha (Dias and Barriga 2006; Cherkashev et al. 2013), and Semyonov (Cherkashev et al. 2010) hydrothermal fields. In most cases, on-land ultramafic-hosted sulfide deposits, if not clearly of primary magmatic origin, are thought to be linked to serpentinization that remobilizes metals from primary silicates (e.g., olivine) into hydrothermal sulfides, if enough H_2S is available (Barrie et al. 1999; Marques et al. 2007 and references therein). However, analysis of vent fluids in active seafloor hydrothermal systems has shown that the concentrations of most elements (e.g., Mn, Zn, Cu, Ag, Ba, Cd, Rb and As) are comparable in ultramafic and basaltic systems, with the exception that fluids from ultramafic-hosted systems have higher concentrations of CH_4, H_2, Co, Ni, Fe and lower Si, Pb, Al, Mg concentrations (Wetzel and Shock 2000; Charlou et al. 2002; Douville et al. 2002; Schmidt et al. 2007). This implies that even in hydrothermal fields hosted in tectonic-related hydrothermal systems, fluids circulate probably also through mafic basements. Allen and Seyfried Jr (2004) further proposed that even for the low-temperature ultramafic-hosted Lost City system, serpentinization likely played an insignificant role accounting for hydrothermal circulation compared with hot lithospheric units and/or near magmatic heat sources, as the chemical compositions (such as Cl, K/Cl, and Na/Cl ratios) of vent fluids from this hydrothermal field are virtually unchanged from the seawater values. In addition, most modern seafloor sulfide deposits are not affected by metamorphism, meaning that the study of modern ultramafic-hosted seafloor hydrothermal systems may provide new insights into the formation of ancient volcanogenic massive sulfide deposits that are spatially related to ultramafic rocks.

Abundant sulfur isotope work has been conducted to investigate the sulfide mineralization mechanisms for modern seafloor hydrothermal systems in a variety of geological settings, such as subduction zones, sediment-covered oceanic ridges near continental margins, and sediment-starved mid-ocean ridges (Shanks III 2001; Hannington et al. 2005; Seal 2006; Peters et al. 2010). Sulfide sulfur in mafic-hosted mid-ocean ridge hydrothermal vents is derived from leaching of basaltic-sulfide and seawater-derived sulfate that is reduced during high-temperature water rock interaction (Ono et al. 2007). However, microbial sulfate reduction during low-temperature serpentinization can provide significant sulfur for sulfide-mineralized systems when they are hosted by mantle peridotites as commonly exposed at slow- and ultraslow-spreading mid-

ocean ridges (Alt and Shanks III 1998, 2011; Alt et al. 2007). The possible sulfur reservoirs for ultramafic-hosted hydrothermal fields therefore have distinct sulfur isotopic compositions, i.e., seawater-derived sulfate with $\delta^{34}S$ values ~ 21‰ (Rees et al. 1978), sulfide derived from mafic and ultramafic rocks with $\delta^{34}S$ values ~ 0‰ (Sakai et al. 1984), and sulfide from microbial sulfate reduction in open environments with significantly ^{34}S depleted sulfur (O'Hanley 1992). Therefore, sulfur isotopes can provide valuable information to identify the sulfur sources and possible reactions during the migration and precipitation of sulfides within hydrothermal systems.

The recently discovered Tianzuo hydrothermal field (27° 57′ S, 63° 32′ E) is an inactive field hosted in ultramafic rocks associated with detachment faults along the SWIR. The sulfides from the Tianzuo hydrothermal field can be generally subdivided into two stages based on their mineral assemblages, with late low-temperature sulfides (pyrite and covellite) replacing or growing around early high-temperature sulfides (isocubanite, pyrrhotine, and sphalerite) (Cao et al. 2018). On the basis of detailed mineralogical studies, this study provides precise sulfur isotopic compositions of sulfides obtained by in situ LA-MC-ICP-MS in order to further understand how sulfide mineralization can develop within ultramafic rocks along amagmatic segments.

Geological setting

SWIR geology

The SWIR separates the African and Antarctic plates from the Bouvet Triple Junction (BTJ; 0° E) in the west to its eastern end at the Rodrigues Triple Junction (RTJ; 70° E) (Fig. 1a). It extends approximately 8000 km with an almost constant spreading rate of ~ 14 mm yr^{-1}, being one of the slowest-spreading ridges globally (Dick et al. 2003; Horner-Johnson et al. 2005). The ridge is characterized by very rugged topography with an axial rift valley and water depths of > 5000 m. It is cut by a series of N–S striking transform faults, which divide it into individual segments with distinct geological characteristics. Bathymetric data reveal a shallow central region between the Prince Edward (35° E) and Gallieni fracture zones (52° 20′ E), with an average depth of ~ 3200 m (Fig. 1a; Sauter et al. 2001; Cannat et al. 2008). The thick oceanic crust indicates a robust magma supply since 10–8 Ma, associated with the Crozet and Marion hotspots (Sauter et al. 2004, 2009; Zhou and Dick 2013; Yang et al. 2017a). The SWIR region between the Melville Fracture Zone (61° E) and RTJ is oriented at ~ 60° to the spreading direction, with no transform faults (Fig. 1b). The easternmost SWIR is characterized by a common departure from isostatic compensation of seafloor topography, pronounced asymmetry in seafloor relief, and a smooth seafloor between the two ridge flanks (Cannat et al. 2003; Sauter et al. 2013). This indicates an anomalously low melt supply and strong tectonism. There has been no obvious magmatic activity for at least 26 Ma in this region (Cannat et al. 2006), distinct from the region between the Prince Edward and Gallieni fracture zones. Compared with other segments of the ridge, the easternmost SWIR has the greatest average water depth (4730 m), thinnest (or missing) crust, and highest basalt $Na_{8.0}$ content, with these features being attributed to lower mantle temperatures and lower degrees of mantle melting (Minshull et al. 2006; Cannat et al. 2008). However, several magmatically robust areas with high relief (e.g., at ~ 61.5° E, 64° E, and 65.5° E) exist along the easternmost SWIR (Fig. 1c), displaying volcanic structures several tens of meters high, with lateral extension for several tens of kilometers.

Geology of the Tianzuo hydrothermal field

The Tianzuo hydrothermal field was discovered during the COMRA DY115-20 cruise by the R/V *Dayangyihao* in 2009 (Tao et al. 2014), and is located in Segment 11 of the SWIR, near the inactive Mt. Jourdanne and active Tiancheng fields (Fig. 1d; Münch et al. 2001; Nayak et al. 2014; Cao et al. 2018; Chen et al. 2018). Further detailed investigations of this hydrothermal site were carried out by the Chinese manned submersible *Jiaolong* during the COMRA DY115-35 cruise conducted by the R/V *Xiangyanghong 9* in 2014–2015. Segment 11 has an hourglass shape extending N–S for > 20 km, with an axial volcanic ridge bounded to the east and west by a non-transform discontinuity (NTD). Along-axis topography in Segment 11 varies within ~ 2700 m, and the crustal thickness is > 6 km at the center with high relief, with an average thickness of ~ 4 km. Maximum crustal thicknesses in adjacent low-relief segments are 2–3 km, indicating focused and variable magmatic accretion (Cannat et al. 2003). The inactive Mt. Jourdanne and adjacent active Tiancheng (which shows low-temperature diffuse flows) hydrothermal fields are located at a volcanic structure along the rift axis, at water depths of 2750 and 2950 m, respectively (Fig. 1c, d). Outcrops in both these fields comprise predominantly basaltic rocks (Münch et al. 2001; Tao et al. 2014; Chen et al. 2018). The Tianzuo hydrothermal field is situated on top of a dome-shaped structure typically associated with oceanic detachment faults (Fig. 1d; Standish and Sims 2010) and outcrops comprise ultramafic rocks, which are distinct from the adjacent fields (Cao et al. 2018; Chen et al. 2018). The Tianzuo field is thus the first confirmed sulfide field hosted by ultramafic rocks and controlled by detachment faults in the SWIR.

The Tianzuo hydrothermal field is located ~ 14 km southeast of the Tianzuo seamount at a depth of 3630 m (Fig. 1d). Hydrothermal activity is likely controlled by the detachment

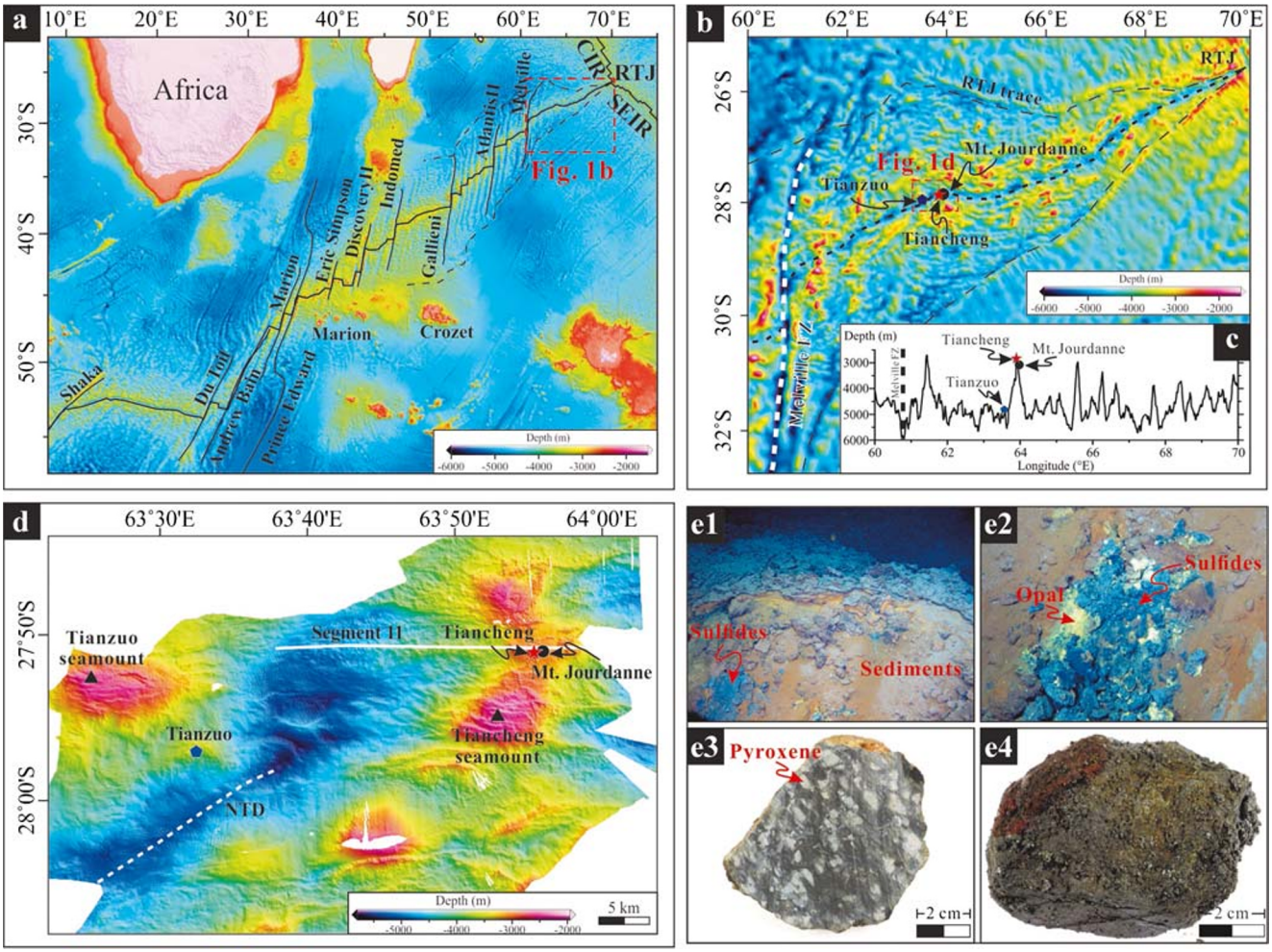

Fig. 1 (a) The geotectonic setting and topography of the Southwest Indian Ridge. (b) The area between the Melville fracture zone and Rodrigues Triple Junction. Ridge segments and non-transform faults are based on Cannat et al. (1999) and Sauter et al. (2001). (c) Along-axis bathymetric profile between 61° E and 69° E (modified from Cannat et al. 2003). (d) Topography of the Tianzuo hydrothermal field and the adjacent Tiancheng and Mt Jourdanne fields from multibeam sonar data. (e1–e2) The red-brown sediments in the Tianzuo hydrothermal field; weathered massive sulfides and opal are commonly observed on the seafloor. (e3–e4) Samples obtained from the Tianzuo hydrothermal field. The altered ultramafic rock in (e3) indicates that the pyroxene phenocrysts are surrounded by serpentine minerals. The sulfides in (e4) are generally cracked and covered by red iron oxide

fault, as in the Logatchev and Rainbow fields (German et al. 1996; Schmidt et al. 2007). The DY115-20 cruise and 88th *Jiaolong* dive found that the main outcrops of the Tianzuo field are altered ultramafic rocks and hydrothermal precipitates (Fig. 1e), with no significant evidence of magmatic activity or typical vent fauna, indicating hydrothermal activity is ancient. Adjacent areas are covered by gray sediments, distinct from the Tianzuo field where opal and red-brown sediments occur over an area of about 800 × 530 m (Fig. 1e1, e2) and where massive sulfide deposits observed on the surface are strongly weathered (Fig. 1e3, e4). Samples analyzed in the present study were collected from the surface of this field by the manned submersible *Jiaolong* during the DY115-35 cruise and 88th *Jiaolong* dive, and mainly include massive sulfide deposits and serpentinized peridotites (Figs. 1e3, e4 and 2a–o). The manned submersible *Jiaolong* dived at the coordinates of 27° 57′ S, 63° 32′ E, exactly located at the eastern part of the Tianzuo hydrothermal field. Four fresh serpentinized peridotite samples were collected from the margin of this field. *Jiaolong* traveled through this field westwards with a total distance of several hundred meters. The field was generally covered by red-brown sediments which most probably resulted from the weathering and oxidization of sulfides. Some strongly weathered ancient sulfide chimneys have been observed standing above these sediments with distinct shapes. Faults and collapses have been observed, with relatively fresh massive sulfides occurring along the fault surfaces. The massive sulfides most likely represent a mound with the diameter of several hundred meters. Three relative fresh massive sulfide samples were collected from the sulfide mound.

Analytical methods

Preliminary SEM and EDS analyses

Thin sections of samples from the Tianzuo hydrothermal field were prepared for mineralogical examination by reflected and transmitted light under a petrographic microscope. Scanning electron microscope (SEM) imaging and energy dispersive system (EDS) element mapping were performed with a Zeiss Supra 55 at the State Key Laboratory for Mineral Deposits Research, Nanjing University, Nanjing, China, with an accelerating voltage of 15 kV and a beam spot size of 60 aperture.

In situ LA-MC-ICP-MS sulfur isotope analysis

Sulfur isotopic compositions of sulfide minerals were determined in situ using a 193-nm ArF excimer laser ablation system (RESOlution S-155) connected to a multi-collector inductively coupled plasma mass spectrometer (Nu Plasma II) at the State Key Laboratory for Geological Processes and Mineral Resources, China University of Geosciences (Wuhan), Wuhan, China. Secondary and back-scattered electron images were used to select spots for analysis, avoiding defects and contamination from different sulfide minerals. The in situ LA-MC-ICP-MS analytical procedure follows the protocol defined in Zhu et al. (2016), and the detailed description of this technique is reported by Mason et al. (2006), Craddock et al. (2008), and Bühn et al. (2012). In brief, helium carrier gas was used at 0.4 L min^{-1} and mixed with Ar (0.8 L min^{-1}) and N_2 (~4 mL min^{-1}) (addition of N_2 eliminates polyatomic interferences such as $^{16}O^{2+}$; Fu et al. 2016). The laser beam diameter was 33 μm, with a repetition rate of 10 Hz for single spot analyses, an energy of 3–4 J cm^{-2}, and the ablation process was set to last for 40 s. An in-house pyrite standard WS-1, consisting of a natural pyrite crystal from the Wenshan polymetallic skarn deposit (Yunnan Province, South China), was used to calibrate the mass bias for S isotopes. The $\delta^{34}S$ composition of WS-1 (1.1 ± 0.2‰) was determined by secondary ion mass spectrometry at the Chinese Academy of Geochemistry, Guangzhou, China (Zhu et al. 2016). Secondary reference material WS-2 pyrite ($\delta^{34}S$ = 2.2‰) was used to monitor the accuracy of the analysis results. All sulfur isotopic compositions are given in the common $\delta^{34}S$ notation as permil difference to the V-CDT-reference (Vienna Canyon Diablo Troilite). The true sulfur isotope ratio of unknown samples was calculated by correction for instrumental mass bias by linear interpolation between the biases calculated from two neighboring standard analyses (WS-1). The internal analytical precision is given as 2 standard deviations (2σ), which is better than ± 0.5‰ (2σ).

Results

Mineralogy of the Tianzuo hydrothermal field

The serpentinized peridotite samples collected from the Tianzuo hydrothermal field are characteristically light-colored showing, in hand specimens, pyroxene crystals surrounded by dark serpentine minerals (Fig. 1e3). Microscopic textures indicated that pyroxene is dominated by clinopyroxene and is cut by veinlets of later serpentine, magnetite, and chrysotile (Fig. 2a). Serpentine minerals, mainly including lizardite and chrysotile, generally retain the pseudomorphic textures after olivine as mesh texture forming a network of veinlets between the relict clinopyroxene, olivine, and minor spinel grains (Fig. 2a–c). These indicate that the source rocks of serpentinized ultramafic rocks were most likely clinopyroxene peridotite. In addition to the abundant magnetite veinlets that crosscut serpentine minerals (Fig. 2a), many subhedral to euhedral magnetite grains occur with a pseudomorphic texture after olivine (Fig. 2d, e), contemporaneous subhedral to euhedral shape hematite is observed coexisting with these magnetite grains (Fig. 2d, e). Minor quartz veinlets also occur within the serpentine minerals, possibly a product of serpentinization.

Sulfide samples collected from the Tianzuo field are yellow–brown in color in hand specimen, and are usually covered by red iron oxide as a result of sulfide weathering (Fig. 1e4). Microscopic observation revealed that sulfides are mainly characterized by major pyrite and isocubanite; and minor sphalerite, pyrrhotite, and covellite, a mineral assemblage of sulfides similar to those described for other hydrothermal fields hosted in ultramafic rocks, such as Logatchev-1, -2, and Rainbow (Lein et al. 2001; Mozgova et al. 2005). These sulfide minerals contain anhedral grains with rare subhedral to euhedral crystals, which are generally disseminated in serpentine-bearing ultramafic rocks, with the exception of covellite and partial pyrite, hosted in quartz veinlets (Fig. 2 and ESM Fig. 1).

Isocubanite disseminated in serpentinite is easily distinguishable from other sulfide minerals in the Tianzuo field. It shows an anhedral shape, brown color, and usually displays grid structures typically resulting from exsolution within other Cu-Fe-sulfides (Fig. 2f, g), such as chalcopyrite, which is further evidenced by the Cu-rich rims around isocubanite, as illustrated by ESM Fig. 1a1-a4. There is no obvious crosscutting relationship between isocubanite, sphalerite, and pyrrhotite (or pyrite with pseudomorphic texture after pyrrhotite), and so precipitation of isocubanite was likely contemporaneous with pyrrhotite and sphalerite crystallization. Isocubanite displays obvious replacement by late pyrite-II (Fig. 2g and ESM Fig. 1a1-a6), and its precipitation must pre-date pyrite-II. The matrix seems to present weathering of serpentine minerals due to the higher

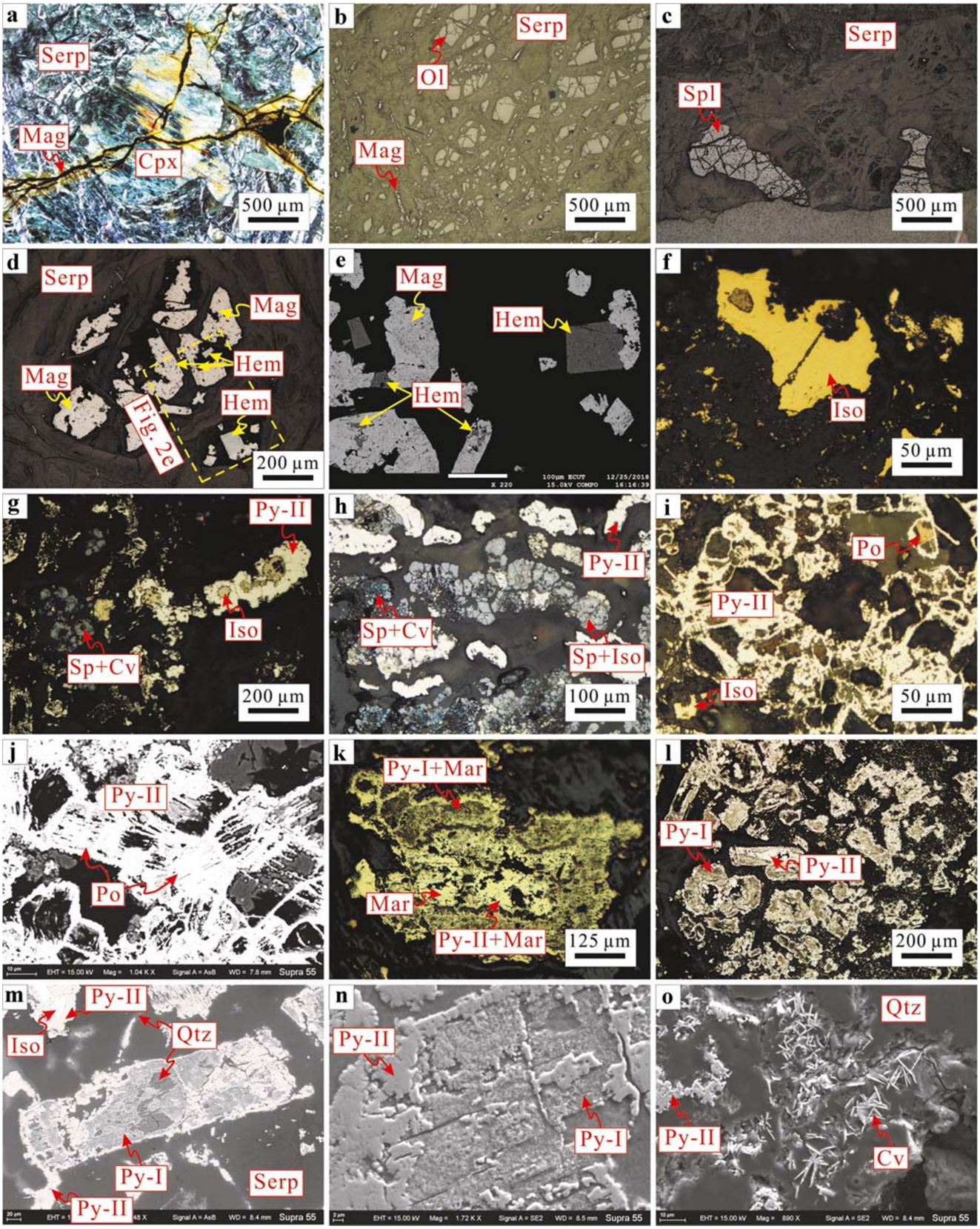
a
Serp
Mag
Cpx
500 μm
b
Serp
Ol
Mag
500 μm
c
Serp
Spl
500 μm
d
Serp
Mag
Hem
Mag
Hem
Fig. 2e
200 μm
e
Mag
Hem
Hem
f
Iso
50 μm
g
Py-II
Iso
Sp+Cv
200 μm
h
Py-II
Sp+Cv
Sp+Iso
100 μm
i
Po
Py-II
Iso
50 μm
j
Py-II
Po
k
Py-I+Mar
Mar
Py-II+Mar
125 μm
l
Py-I
Py-II
200 μm
m
Py-II
Iso
Qtz
Py-I
Py-II
Serp
n
Py-II
Py-I
o
Qtz
Py-II
Cv

◀ **Fig. 2** Microscopic images of samples collected from the Tianzuo hydrothermal field. **a** Partially serpentinized peridotite showing clinopyroxene phenocrysts surrounded by serpentine minerals, both of which are crosscut by late magnetite veinlets (cross-polarized light). **b** Olivine altered as serpentine minerals with the mesh texture consisting of relict olivine surrounded by a network of serpentine veinlets between the olivine grains (reflected light). **c** Spinel surrounded by serpentine minerals (reflected light). **d** Magnetite coexisting with hematite and occurring as fillings in holes of serpentine minerals (reflected light). **e** Subsection of Fig. 2 d, showing hematite with subhedral to euhedral shape, or occurring as an exsolution within magnetite (back-scattered electron image). **f** Isocubanite with typical grid structure disseminated in serpentine minerals (reflected light). **g** Isocubanite replaced by pyrite-II; sphalerite replaced by late covellite (reflected light). **h** Sphalerite with isocubanite exsolution (reflected light). **i**, **j** Pyrite-II rims retaining a pseudomorphic texture after pyrrhotite (**i** reflected light, **j** back-scattered electron image). **k** Pyrite-I replacing pyrrhotite, showing pseudomorphic textures after pyrrhotite, which was further replaced by pyrite-II; marcasite can be observed coexisting with pyrite-I or included in pyrite-II as relicts (reflected light). **l**–**n** Fine-grained pyrite-I filling the outline of early pyrrhotite with quartz, and replaced by late pyrite-II (**l** reflected light, **m** back-scattered electron image, **n** secondary electron image). **o** Covellite occurred in quartz as lamellae or fibrous (secondary electron image). Mag, magnetite; Serp, serpentine; Cpx, clinopyroxene; Ol, olivine; Spl, spinel; Hem, hematite; Iso, isocubanite; Py, pyrite; Sp, sphalerite; Cv, covellite; Po, pyrrhotite; Mar, marcasite; Qtz, quartz

concentrations of Si and Mg, as illustrated by EDS element mapping (ESM Fig. 1a5-a6). Experimental studies of the phase relationships of reactions in the Cu-Fe-S and Fe-S systems indicate that at temperatures of > 335 °C, isocubanite begins to crystallize with chalcopyrite, pyrite, and pyrrhotite (Lusk and Bray 2002). Isocubanite was thus likely precipitated during the early high-temperature phase of the Tianzuo field.

Sphalerite is rare in the Tianzuo samples, as indicated by SEM imaging and EDS element mapping (ESM Fig. 1b-c). It is generally anhedral, gray in color, and usually contains abundant isocubanite or, conversely, it is included in isocubanite as exsolution lamellae (Fig. 2h and ESM Fig. 1b1-b6). Fewer subhedral sphalerite grains can also be found contained in serpentine minerals in this field (ESM Fig. 1c1-c3). This mineral is usually replaced by late pyrite-II similar to isocubanite, indicating that it precipitated with isocubanite during an early high-temperature phase.

Pyrrhotite is rare in Tianzuo sulfide samples, and is usually included in pyrite-II, with an anhedral shape, as a relict, which was replaced by late pyrite-II (Fig. 2i, j and ESM Fig. 1d1-d3). In addition, pyrrhotite plates can also be completely replaced by pyrite-I, resulting abundant pseudomorphic textures after pyrrhotite. Sometimes, pyrite-I crystals were absent due to strong weathering, resulting in abundant holes surrounded by pyrite-II rims with pseudomorphic textures after pyrrhotite (Fig. 2i–n and ESM Fig. 1d-e). Pyrite-I and -II replacing or growing around pyrrhotite displays pseudomorphic textures after pyrrhotite, indicating that Tianzuo field was originally enriched in pyrrhotite that was almost completely replaced by late pyrite-I and -II during the late low-temperature phase, resulting in few pyrrhotite relicts in pyrite-II and abundant pseudomorphic textures (Fig. 2j–n and ESM Fig. 1e1-e6).

Pyrite is the most abundant sulfide phase in Tianzuo field and it is either hosted in serpentine minerals or coexists with quartz (Fig. 2g–n and ESM Fig. 1e1-e6). Based on its morphology, pyrite can be subdivided into two types, i.e., pyrite-I coexisted with marcasite as colloform, retaining pseudomorphic textures after pyrrhotite and creating a turbid appearance in thin section (Fig. 2k–n); pyrite-II with crystals that have typically grown around and replace early isocubanite, sphalerite, pyrrhotite, and pyrite-I, or are present as individual grains in quartz veinlets, with no inclusions visible in microscopic examination (Fig. 2g–n and ESM Fig. 1a, d, e). The matrix containing pyrite-I is also abundant in serpentine minerals, while that containing pyrite-II is most likely quartz as indicated by EDS element mapping (ESM Fig. 1e5-e6). Marcasite relicts can be also observed retained in pyrite-II (Fig. 2k). Marcasite is unstable and precipitates at relatively low temperatures (< 200 °C) and low pH (< 4.5). It undergoes transformation to pyrite at temperatures of > 350 °C (Fleet 1970). Pyrite-I and -II in the Tianzuo hydrothermal field usually replaced early minerals, including isocubanite, sphalerite, and pyrrhotite, suggesting that they precipitated after these minerals and crystallized during a low-temperature phase. This is particularly evident for pyrite-II, which also replaced pyrite-I, indicating that this mineral precipitated later than pyrite-I (Fig. 2k–n).

Covellite is another low-temperature sulfide mineral found in Tianzuo sulfide samples. The atom ratios of Cu/S obtained by EMPA are 1:1 (Cao et al. 2018). It is blue in color, usually replacing sphalerite with an anhedral morphology (Fig. 2g–h) or occurring in quartz veinlets as lamellae or fibers (Fig. 2o and ESM Fig. 1f1-f6).

On the basis of these observations, it is concluded that sulfide mineralization in the Tianzuo hydrothermal field occurred in two stages, i.e., an early high-temperature stage (> 335 °C; isocubanite, sphalerite, and pyrrhotite) and a late low-temperature stage (< 200 °C; pyrite-I, -II, and covellite).

Sulfur isotopic composition of sulfide phases

Sulfur isotopic compositions of 81 individual sulfide minerals were determined, including 26 isocubanite, 8 sphalerite, 32 pyrite-I, and 15 pyrite-II samples. Results are presented in ESM Table 1 and illustrated in Fig. 3 a. The grain sizes of pyrrhotite and covellite were too small for such analyses. Sulfide minerals from the Tianzuo hydrothermal field display a large variation in $\delta^{34}S$ values. Isocubanite has the least variability in $\delta^{34}S$, with values of 9.6 to 12.2‰; sphalerite has the

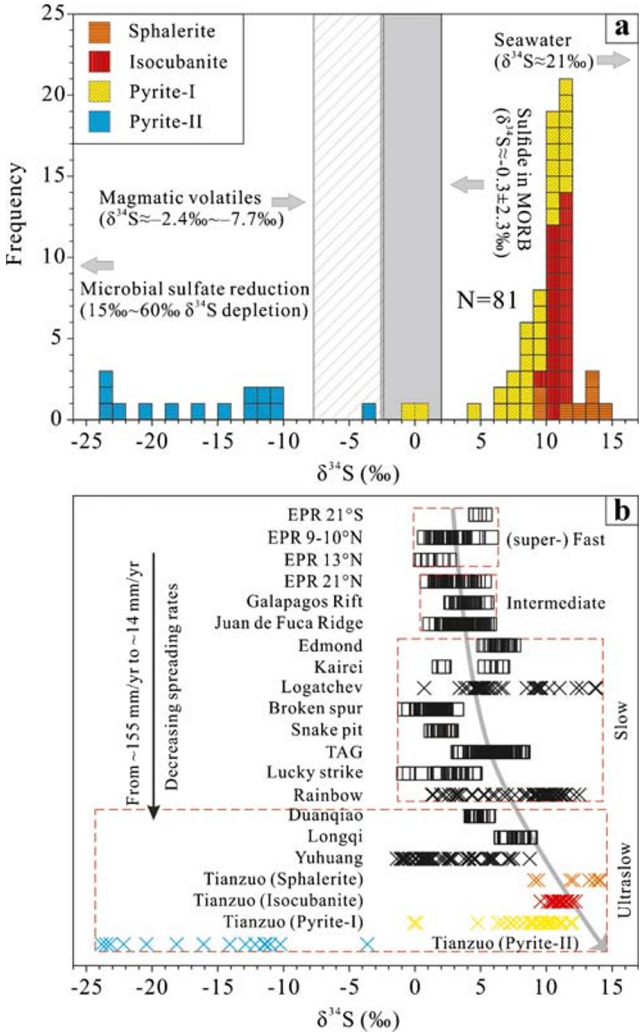

Fig. 3 **a** Frequency distribution of $\delta^{34}S$ values for sulfides from the Tianzuo hydrothermal field. **b** Range of $\delta^{34}S$ values for sulfides from modern sediment-starved ridges, showing that sulfides hosted in ultramafic rocks (cross) have wider ranges than those hosted in basaltic rocks (square). Data sources: Seawater (Rees et al. 1978), sulfides in MORB (Sakai et al. 1984), magmatic volatiles based on the sulfides (native sulfur) from Lau Basin (Herzig et al. 1998), East Pacific Rise (EPR) 21° S and EPR 13° N (Ono et al. 2007), EPR 9°–10° N (Ono et al. 2007; Rouxel et al. 2008), EPR 21° N (Woodruff and Shanks III 1988); Galapagos Rift (Knott et al. 1995); Juan de Fuca Ridge (Shanks III and Seyfried Jr 1987; Hannington and Scott 1988); Edmond and Kairei (Wang 2012; Zeng et al. 2016); Logatchev (Bogdanov et al. 1997; Rouxel et al. 2004; Zeng et al. 2016); Broken Spur (Duckworth et al. 1995; Butler et al. 1998); Snake Pit (Kase et al. 1990); Trans-Atlantic Geotraverse (TAG; Herzig et al. 1998; Knott et al. 1998; Zeng et al. 2016); Lucky Strike (Rouxel et al. 2004; Ono et al. 2007); Rainbow (Lein et al. 2001; Rouxel et al. 2004); Yuhuang (Liao et al. 2018); Duanqiao (Yang et al. 2017b); Longqi (Ye 2010). Spreading rates of mid-ocean ridges are based on Baker et al. (1996) and Hannington et al. (2005, 2010)

highest value, ranging from 9.1 to 14.1‰; pyrite-I has variable and generally positive $\delta^{34}S$ values of − 0.1 to 12.0‰; and pyrite-II has the lowest and most variable values of − 23.8 to − 3.6‰.

Discussion

Potential sulfur sources for modern seafloor hydrothermal fields

The $\delta^{34}S$ values of sulfide minerals in modern sediment-starved ridge hydrothermal systems typically range from 1 to 7‰ (Shanks III et al. 1995; Shanks III 2001; Hannington et al. 2005; Seal 2006; Peters et al. 2010). In mid-ocean ridge hydrothermal systems, sulfur forming hydrothermal sulfides are derived from different sources, i.e., (1) magmatic (including degassing processes), (2) leaching from the ocean basement rocks and sediment covers, (3) thermochemical reduction of seawater sulfate, and (4) remobilization of sulfur produced by microbial sulfate reduction. Each of these sources has distinctive sulfur isotopic signatures (Ohmoto and Rye 1979; Seal 2006 and references therein). At magmatic temperatures (higher than 400 °C), sulfur at deeper zones of the hydrothermal system has $\delta^{34}S$ values close to 0‰, as SO_2 is totally reduced to H_2S and sulfides forming from these fluids (Herzig et al. 1998). However, at the temperatures below 350–400 °C, the $\delta^{34}S$ values will disproportionate rapidly according to the disproportionation reaction: $4SO_2(aq) + 4H_2O(g) = H_2S(aq) + 3H^+ + 3HSO_4^-$, the $\delta^{34}S$ values of the sulfides precipitated from these fluids will be < 0‰ and the $\delta^{34}S$ values of the sulfate derived from the same fluids will be > 0‰ and generally lower than seawater (Ohmoto and Rye 1979 and references therein). For example, sulfides (native sulfur) and barite from the Hine Hina hydrothermal field, Lau Basin, have $\delta^{34}S$ values ranging from − 7.7 to − 2.4‰ and 16.1 to 16.7‰, respectively (Herzig et al. 1998). According to the model of Janecky and Shanks III (1988), simple adiabatic mixing associated with seawater-basalt interactions produces H_2S with a maximum $\delta^{34}S$ value of 4.5‰, whereas H_2S produced through thermochemical reduction of modern seawater sulfate, through interaction with magnetite and fayalite, has $\delta^{34}S$ values which can fractionate by a scale up to 21‰ (Ohmoto et al. 1983). Anhydrite precipitated from the pristine seawater has the $\delta^{34}S$ value as the same as seawater (~ 21‰; Rees et al. 1978; Chiba et al. 1998; Herzig et al. 1998; Zeng et al. 2016). In contrast, H_2S produced through dissolution of biogenic sulfides in sedimentary rocks has negative $\delta^{34}S$ values reflecting microbial sulfate reduction (Canfield and Teske 1996; Ohmoto and Goldhaber 1997; Alt and Shanks III 1998, 2011; Allen and Seyfried Jr 2004; Alt et al. 2007), although questions remain about the magnitude of sulfur isotope fractionation during microbial sulfate reduction (Rouxel et al. 2008); this microbial sulfate reduction may cause sulfate–sulfide fractionation of 15 to 60‰ (Goldhaber and Kaplan 1975; Canfield and Teske 1996; Detmers et al. 2001; Wortmann et al. 2001; Canfield 2002).

The $\delta^{34}S$ values of hydrothermal sulfides precipitated in sediment-starved ridges with a range of spreading rates and

hosted in basaltic rocks varies in a narrow range (1 to 7‰) (Fig. 3b; Shanks III et al. 1995; Shanks III 2001; Hannington et al. 2005; Seal 2006; Peters et al. 2010; Zeng et al. 2016) and mainly represent sulfur leached from basaltic substrate, with little contribution from inorganically reduced seawater sulfate. Increasing contributions of reduced seawater sulfate and higher $\delta^{34}S$ values occur as ridge spreading rate decreases (Fig. 3b), reflecting equilibration of hydrothermal fluids with rocks that have already undergone a long history of seawater–rock interaction (Shanks III 2001). Sulfides hosted by ultramafic rocks, as in the Logatchev, Rainbow, and Tianzuo hydrothermal fields, or closely associated with these rocks as in the Yuhuang field (Liao et al. 2018), have greater $\delta^{34}S$ variability than those hosted in basaltic rocks (Fig. 3b). This feature applies especially to the Tianzuo field, where sphalerite has the highest (14.1‰) and pyrite-II has the lowest (− 23.8‰) $\delta^{34}S$ values found to date in sediment-starved ridges, with these minerals representing high- and low-temperature mineralization phases, respectively. Neither basaltic magmatism nor seawater-basalt interactions can generate reduced H_2S with such extremely positive and negative $\delta^{34}S$ values as mentioned above, thus, we favor that thermochemical reduction of early precipitated anhydrite and leaching of sulfides in the wall rocks produced by microbial sulfate reduction most likely have isotopically played an important role for the sulfide mineralization in this Tianzuo field.

Possible early anhydrite precipitation in the Tianzuo hydrothermal field

In the Tianzuo hydrothermal field, sulfide minerals are hosted in serpentine-bearing ultramafic rocks where fractures are widely developed, in accordance with the SWIR being controlled mainly by tectonism rather than magmatism (Standish and Sims 2010; Tao et al. 2020). Early stage sulfide minerals, including isocubanite and sphalerite, are isotopically heavier than those from other sediment-starved systems, especially for sulfides hosted in basaltic rocks (ESM Table 1; Fig. 3). H_2S from the deep reaction zone in the Tianzuo field is thus isotopically heavier than that from other sediment-starved systems. $\delta^{34}S$ values for the two early sulfide minerals are as high as 14.1‰ (ESM Table 1), with such heavy values requiring the addition of sulfur from seawater sulfate, and limited volcanogenic and/or microbial reduction contributions (Lein et al. 2001; Shanks III 2001; Hannington et al. 2005; Seal 2006; Ono et al. 2007; Peters et al. 2010). It seems, therefore, that reduction of aqueous sulfate and/or reduction of anhydrite must have occurred in the deep reaction zone of this hydrothermal system. Seawater contains ~ 10 mmol/kg Ca^{2+} and ~ 28 mmol/kg SO^{2-}_4 and anhydrite precipitates from pristine seawater upon heating above 150 °C in the low-temperature recharge zone, only a small proportion (< 1 mmol/kg) sulfate enters to the deep high-temperature (> 250 °C) reaction zone (Woodruff and Shanks III 1988; Sleep 1991), this indicates that if the temperature in the pathway between recharge and reaction zones was low enough, seawater sulfate could reach the reaction zone, leading to anhydrite precipitation at depth (Lowell and Yao 2002; Lowell et al. 2003; Ono et al. 2007).

The dissolution of anhydrite precipitated during an early low-temperature phase may explain the heavy isotopic composition of sulfide minerals formed during the subsequent high-temperature sulfide mineralization, such as isocubanite and sphalerite, in the Tianzuo hydrothermal field. Although the formation of oceanic core complexes means that at least part of the oceanic lithosphere formed at slow- and ultraslow-spreading centers comprises peridotite with gabbroic intrusions in varying proportions (Ranero and Reston 1999; Lowell and Rona 2002; Ildefonse et al. 2007; Escartin et al. 2008), there is no evidence that earlier sulfides existed before isocubanite and sphalerite in this Tianzuo hydrothermal field. In addition, $\delta^{34}S$ values of isocubanite and sphalerite from this field fall within a narrow range (9.1 to 14.1‰), meaning that the formation of these two sulfide minerals most likely dominated by one major gabbroic intrusion event rather than multiple magmatic activities, as the latter most likely will result in multi-stage sulfide mineralization overlapped with different $\delta^{34}S$ values (Woodruff and Shanks III 1988), especially with the involvement of seawater sulfate, so we favor that there were probably no early high-temperature gabbroic intrusions which have significantly contributed to the sulfide mineralization in this Tianzuo hydrothermal field. It appears likely, therefore, that hydrothermal circulation was initially of low-temperature, dominated by seawater, and driven more notoriously by the exothermic serpentinization of ultramafic rocks. In fact, the decreasing solubility of anhydrite and other sulfate minerals as temperature increases leads to their removal from seawater by precipitation during heating associated with downwelling (Bischoff and Seyfried Jr 1978; Seyfried Jr and Bischoff 1981; Shanks III et al. 1995), as illustrated in Fig. 4a. Although the studies about the faults in the Tianzuo field were limited, fractures with extreme depths (13 ± 2 km), which are even deeper than the other mafic- and ultramafic-hosted hydrothermal fields, such as Trans-Atlantic Geotraverse (TAG) and Logachev-1 on the MAR, can well developed in this ultraslow-spreading SWIR (Tao et al. 2020). The anhydrite precipitated in the deep fractures during this early low-temperature phase can be dissolved into the subsequent high-temperature hydrothermal circulation, which has an isotopically significant contribution for the formation of isocubanite and sphalerite, as discussed below.

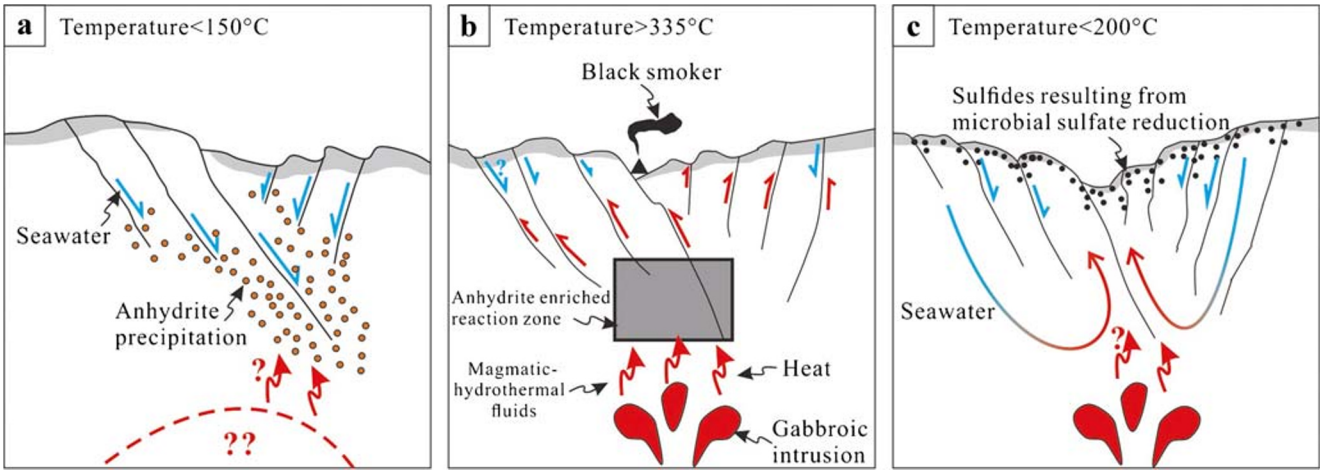

Fig. 4 Cartoon showing the sulfide formation processes in the Tianzuo hydrothermal field. **a** Anhydrite precipitated in the reaction zone during an earlier phase of low-temperature hydrothermal circulation. **b** Gabbroic intrusion provided sufficient heat to drive high-temperature hydrothermal circulation; earlier precipitated anhydrite is available for high-temperature sulfate reduction; all high-temperature and isotopically heavier sulfides precipitated, including isocubanite, sphalerite, and pyrrhotite. **c** Seawater-dominated, low-temperature, hydrothermal circulation while the magma chamber is cooling; sulfur from microbial sulfate reduction is the predominant sulfur source for late sulfide minerals, including pyrite-II and most probably covellite

High-temperature phase sulfide mineralization in the Tianzuo hydrothermal field

Previous studies have shown that venting in modern seafloor hydrothermal systems, such as the TAG, Edmond, Kairei, and Duanqiao fields, has been intermittent in the past (Lalou et al. 1998; Chiba et al. 1998; Rouxel et al. 2008; Wang 2012; Yang et al. 2017b), implying that hydrothermal discharge through major fracture systems may be reactivated. If high-temperature activity was reactivated after a previous low-temperature phase, seawater-derived sulfate (in the form of anhydrite) would be available as a source of sulfur, in addition to basaltic sulfur (Janecky and Shanks III 1988). With abundant sulfate, sulfate sulfur would be reduced by reaction with magnetite and/or fayalite in ultramafic rocks and incorporated into the hydrothermal fluid, such as $4H^+ + 2SO^{2-}{}_4 + 12Fe_3O_4 = 18Fe_2O_3 + FeS_2 + 2H_2O$ (Gow et al. 1994). Abundant hematite and magnetite coexisting in the serpentine minerals further support this hypothesis for Tianzuo hydrothermal field (Fig. 2d, e). Potential sources of heat include magmatism, mantle upwelling, and serpentinization (German and Lin 2004; Lowell and Rona 2002), with serpentinization previously being considered the major source (McCaig et al. 2007). However, heat balance models predict that heat released during serpentinization of peridotites may result in a wide range of hydrothermal venting temperatures, while temperatures of hydrothermal fluids triggered by this process are up to only 40–75 °C (Lowell and Rona 2002). Furthermore, serpentinization cannot explain the abundance of rare earth elements, Ba, and Si in hydrothermal fluids (Douville et al. 2002). Gabbroic intrusions are therefore likely sources of heat and elements key for the formation of sulfides, even in hydrothermal fields with sulfides hosted in ultramafic rocks (Wetzel and Shock 2000). Movement along detachment faults may exhume gabbros and even peridotites, both of which are features of modern oceanic core complexes (Ranero and Reston 1999). However, in the Tianzuo field, sulfide minerals precipitated during a high-temperature phase, including isocubanite and sphalerite, have the highest and most uniform $\delta^{34}S$ values (Fig. 3a), indicating that sulfur was derived from a homogeneous source with high $\delta^{34}S$ values before precipitation as Fe, Cu, and Zn sulfides.

For the seafloor hydrothermal systems, precipitation of anhydrite is probably important (Sleep 1991; Lowell and Yao 2002; Lowell et al. 2003), and numerous studies have shown the presence of anhydrite in the serpentine ultramafic rocks (Alt and Shanks III 1998, 2011; Allen and Seyfried Jr 2004; Alt et al. 2007). As mentioned above, the gabbroic intrusion most likely has provided sufficient heat driving the hydrothermal circulation where high-temperature phase (> 335 °C) isocubanite, sphalerite, and pyrrhotite precipitated in Tianzuo hydrothermal field; this means that in the high-temperature reaction zone, the hydrothermal fluids can gain reduced sulfur (H_2S) from reduction of seawater-derived anhydrite in addition of the leaching of sulfides from the wall rocks (e.g., gabbros and peridotite). The models previously used to interpret the various $\delta^{34}S$ values of sulfides in the seafloor hydrothermal systems including (1) the anhydrite buffer model (Ohmoto et al. 1983), (2) disproportionation of SO_2 (Ohmoto and Rye 1979; Herzig et al. 1998), and (3) two-component mixing (Janecky and Shanks III 1988; Shanks III 2001). The anhydrite buffer model suggests that the majority

of hydrothermal sulfides ultimately derived from seawater-derived sulfate, the $\delta^{34}S$ values of these sulfides essentially reflect the fractionation factor between sulfate (SO^{2-}_4) and sulfide (H_2S). The isotope fractionation factors between sulfate and sulfide are 21 and 15‰ at 300 °C and 400 °C (Ohmoto et al. 1983), respectively, which can explain why the hydrothermal sulfides in the seafloor hydrothermal system have the $\delta^{34}S$ values generally range from 1 to 7‰ (seal 2006 and the references therein). However, this model cannot explain the extremely high $\delta^{34}S$ values for the isocubanite and sphalerite from the Tianzuo hydrothermal field (9.1 to 14.1‰). The disproportionation of SO_2 means that the SO_2 in the volcanic gases will disproportionate rapidly into reduced H_2S and oxidized SO^{2-}_4 when temperatures below 300–400 °C, with the sulfides precipitated in the hydrothermal fluids have low $\delta^{34}S$ values (< 0‰) and the sulfates have relative high $\delta^{34}S$ values (> 0‰). This model was generally used to explain the formation of those sulfides occurred in the arc/back arc environments with low $\delta^{34}S$ values and characteristic acid-sulfate alteration assemblages (e.g., alunite/barite-pyrite in the Lau Basin; Herzig et al. 1998). The isocubanite and sphalerite have extremely high $\delta^{34}S$ values and sulfates are absent in the Tianzuo hydrothermal field; the influence of disproportionation of SO_2 therefore can be removed from this field. Thus, for the Tianzuo hydrothermal field, the $\delta^{34}S$ values of isocubanite and sphalerite most likely reflect two-component mixing between seawater-derived sulfate ($\delta^{34}S \approx$ 21‰) and wall rocks/gabbroic intrusion-derived sulfide ($\delta^{34}S \approx 0$‰). Based on this two component mixing model, the highest $\delta^{34}S$ value of sulfides form the Tianzuo hydrothermal field ($\delta^{34}S = 14.1$‰) indicates that about 33% of H_2S was derived from leaching of sulfides from wall rocks/gabbroic intrusion, and the seawater-derived sulfates have provided the other 67% of H_2S; the gabbroic intrusion most likely has a significant contribution to the sulfur forming these high-temperature phase sulfides in addition of the abundant heat as mentioned before.

The Tianzuo hydrothermal field is located about 35 km to the southwest of Mt. Jourdanne hydrothermal field (Fig. 1d). Previous studies have shown that abundant galena occurred in the sulfide assemblages within the Mt. Jourdanne field, and the sulfides from this field have high concentrations for the elements Pb (up to 3.54 wt%), As (up to 0.57 wt%), Cd (up to 0.22 wt%), and Ag (up to 0.13 wt%) (Münch et al. 2001; Nayak et al. 2014). Since the enrichment of galena and those elements Pb, As, Cd, and Ag are generally observed in the arc/back arc environments associated with felsic magmas rather than sediment-starved oceanic ridges associated with basalts, Nayak et al. (2014) proposed that within the Mt. Jourdanne seamount structure, isolated bodies of more felsic rocks may provide a source for the abundant Pb, As, Cd, and Ag found in its sulfides. Therefore, another explanation for the isotopically heavier sulfides in the Tianzuo field may be the occurrence of granitic rocks in the area. Such as rocks of granitic composition have already been found in the Central Indian Ridge near the Agro Fracture Zone (Engel and Fisher 1975) and a range of volcanic rocks, from andesite to rhyodacite, has been recovered from the Galapagos Spreading Center (Shibata et al. 1979). Granitoids have an average $\delta^{34}S$ value of 1.0 ± 6.1‰, with a range of − 11 to 14.5‰, reflecting variable assimilation or partial melting of either pyritic sedimentary rocks with low $\delta^{34}S$ values or evaporites with high $\delta^{34}S$ values (Ishihara and Sasaki 1989). Granites and syenites from southern India have $\delta^{34}S$ values of 2.5 to 14.5‰ (Santosh and Masuda 1991), which are approximatively close to those of isocubanite and sphalerite from Tianzuo field. However, sulfides such as isocubanite and pyrite are depleted in these elements, including Pb, As, Cd, and Ag (Cao et al. 2018), and the Tianzuo field lacks galena (abundant in the Mt. Jourdanne field), with no significant evidence of granitic rocks. The influence of granitic rocks is thus precluded, with reduction of anhydrite (deposited during early low-temperature hydrothermal circulation through deep fractures) in the high-temperature phase being favored as the main source of isotopically heavy sulfur in isocubanite and sphalerite. Hydrothermal fluids would have been mixed in the reaction zone and heated by the gabbroic intrusion; hot fluids with homogeneous sulfur isotopic compositions would then ascend and be exhaled on the seafloor, resulting in sulfide deposition during the high-temperature phase (Fig. 4b). When high-temperature activity declined, low-temperature seawater-derived fluid may have eventually dominated hydrothermal fluid circulation again. Pyrite-I, -II, and covellite would have precipitated during this low-temperature phase.

Low-temperature phase sulfide mineralization in the Tianzuo hydrothermal field

Pyrite-II has the lowest and most variable $\delta^{34}S$ values (− 23.8 to − 3.6‰) of sulfide minerals in the Tianzuo field, with significant signs of sulfate-reducing microbial activity. Such low $\delta^{34}S$ values have not previously been reported for sulfides in sediment-starved ridges, but are commonly observed in sediment-covered ridges and back arc basins (e.g., Shanks III 2001; Hannington et al. 2005; Seal 2006; Ono et al. 2007; Peters et al. 2010), such as the Kebrit, Shaban and Atlantis II Deeps, Red Sea (Zierenberg and Shanks III 1988), Lau Basin (Herzig et al. 1998), Guaymas Basin (Peter and Shanks III 1992), and Middle Valley (Zierenberg 1994). Pyrite-II $\delta^{34}S$ values indicate some influence of magmatic sulfur, and a larger contribution of microbial action than in basalt-dominated systems. In addition to detachment faults, the widely developed fractures in the Tianzuo field may have also resulted from expansion during serpentinization of minerals in ultramafic rocks such as olivine, where a 40 to 50% volume increase may occur (O'Hanley 1992). With the stable

permeability of the ridge, hydrothermal fluid pathways may exist long after high-temperature hydrothermal circulation has ended. Furthermore, compared with the initial low-temperature stage when the anhydrite precipitated, the high-temperature circulation provided enough materials for life to flourish in the hydrothermal field, probably including sulfate-reducing bacteria, with numerous sulfides containing microbially reduced sulfur, which precipitated when temperatures declined.

As mentioned above, disproportionation of SO_2 can also generate reduced H_2S enriched in ^{32}S (Ohmoto and Rye 1979; Herzig et al. 1998). However, this reaction most likely happened under arc/back arc environment with felsic magmatism, and the reported $\delta^{34}S$ values of H_2S range from −2.4 to −7.7‰ in the Lau Basin (Herzig et al. 1998), which is much higher than those of the pyrite-II (−23.8 to −3.6‰) from this Tianzuo field. In addition, disproportionation of SO_2 will result in acid-sulfate alteration assemblages which are absent in the Tianzuo field (Herzig et al. 1998), this reaction therefore can be removed when pyrite-II precipitated. Although significant microbial sulfate reduction has been generally observed in the sediments covered hydrothermal fields, previous studies have shown that microbial sulfate reduction was also widespread in the altered basalts and mantle exposed at the seafloor along the sediment-starved ridges, as indicated by that sulfides contained in these rocks have significantly negative $\delta^{34}S$ values (Canfield and Teske 1996; Alt and Shanks III 1998, 2011; Allen and Seyfried Jr 2004; Alt et al. 2007). In fact, the uptake of sulfur by serpentinites in oceanic basement is comparable to or greater than that by comparable volumes of mafic oceanic crust, as the microbial communities can be supported by the hydrogen and methane generated by both the alteration of basalts and serpentinization reactions of ultramafic rocks with the temperature up to 120 °C (Canfield 2002; Schwarzenbach et al. 2012). Pyrite-I, -II, and covellite in the Tianzuo field are low-temperature phase sulfides (< 200 °C), meaning that the precipitation of these three sulfides were not significantly influenced by high-temperature gabbroic intrusions, this enabled the microbial reduction of seawater sulfate and addition of low-$\delta^{34}S$ sulfide to the wall rocks. Therefore, it is likely that the leaching of sulfide minerals produced by microbial sulfate reduction was the main source of sulfur for pyrite-II during the late low-temperature phase, with the influence of isotopically heavy residual sulfate and volcanogenic sulfur being limited (Fig. 4c).

Pyrite-I has similar variability, but much higher $\delta^{34}S$ values (−0.1 to 12.0‰) than pyrite-II (Fig. 3 and ESM Table 1), and displays obvious mixing of sulfur sources. As indicated by the mineralogy of sulfides, pyrite-I has obvious pseudomorphic texture after pyrrhotite (Fig. 2k–n). The influence of pyrite-II on pyrite-I is difficult to evaluate as it usually grows around pyrite-I (Fig. 2k–n and ESM Fig. 1e1-e6), but the generally positive $\delta^{34}S$ values of pyrite-I indicate a limited contribution of sulfur from microbial sulfate reduction. One mixing end-member of pyrite-I is likely dominated by volcanogenic sulfur leaching from the wall rocks, and the other by thermochemical reduction of earlier formed sulfate during the high-temperature phase when pyrrhotite precipitated. As with isocubanite and sphalerite, the high $\delta^{34}S$ values of pyrite-I were likely inherited from sulfur isotopic compositions of original pyrrhotite.

Conclusions

Sulfides hosted in serpentinized ultramafic rocks in the Tianzuo hydrothermal field, in an amagmatic segment of the ultraslow-spreading SWIR, include minerals from different formation phases. These include high-temperature isocubanite, sphalerite, and pyrrhotite, and low-temperature pyrite and covellite. Pyrite may be subdivided into pyrite-I and -II based on morphology, with the former displaying an obvious pseudomorphic texture after pyrrhotite. Isocubanite and sphalerite have high and uniform $\delta^{34}S$ values, with thermochemical reduction of sulfate precipitated during early phase low-temperature hydrothermal circulation contributing sulfur for these sulfide minerals, and probably for the original pyrrhotite. Gabbroic intrusions provided heat for driving the subsequent high-temperature hydrothermal fluid circulation, creating a homogeneous sulfur environment in the reaction zone. Pyrite-I, -II, and covellite precipitated when temperature declined. Pyrite-I has variable and generally positive $\delta^{34}S$ values, and its sulfur was inherited from the original pyrrhotite through thermochemical reduction of sulfate, mixed with some additional volcanogenic sulfur. Pyrite-II has the lowest and most variable $\delta^{34}S$ values, and displays significant signs of microbial sulfate-reducing activity, with the leaching of sulfide minerals from wall rocks with seawater being the main sulfur source for this mineral. Intermittent magmatism, together with persistent high permeability, probably contributed to the formation of sulfides in the Tianzuo hydrothermal field, and this may also be the mechanism for the formation of sulfides hosted in other ultramafic rocks at slow- and ultraslow-spreading ridges.

Acknowledgments We are grateful to Dr. Crystal LaFlamme, an anonymous reviewer, Dr. Marco Fiorentini (Editor) and Dr. Bernd Lehmann (Editor-in-Chief) for their thoughtful reviews and constructive comments.

Funding This work is financially supported by the National Key Research and Development Program of China under contract nos. 2017YFC0306603, 2018YFC0309901, 2016YFC0304905, and 2018YFC0309902; the National Science Foundation for Young Scientists of China (Grant Nos. 41803037 and 41806076); the Foundation for Young Scientists of Jiangsu Province (Grant No. BK20180511); the Fundamental research Funds for the Central Universities (Grant Nos. 2017B03314 and 2017B04514); the COMRA Major Project under contract nos. DY135-S1-1-01 and DY135-S1-1-02;

the Zhejiang Provincial Natural Science Foundation of China (Grant No. LQ16D060008), Scientific Research Fund of the Second Institute of Oceanography (Grant No. JG1609), Macao Science and Technology Development Fund (FDCT-002/2018/A1), China Postdoctoral Science Foundation (2019M652043), and Open Research Fund Program of Key Laboratory of Metallogenic Prediction of Nonferrous Metals and Geological Environment Monitoring (Central South University), Ministry of Education (2019YSJS03).

References

Allen DE, Seyfried WE Jr (2004) Serpentinization and heat generation: constraints from Lost City and Rainbow hydrothermal systems. Geochim Cosmochim Acta 68(6):1347–1354

Alt JC, Shanks WC III (1998) Sulfur in serpentinized oceanic peridotites: serpentinization processes and microbial sulfate reduction. J Geophys Res 103(B5):9917–9929

Alt JC, Shanks WC III (2011) Microbial sulfate reduction and the sulfur budget for a complete section of altered oceanic basalts, IODP Hole 1256D (eastern Pacific). Earth Planet Sci Lett 310:73–83

Alt JC, Shanks WC, Bach W, Paulick H, Garrido CJ, Beaudoin G (2007) Hydrothermal alteration and microbial sulfate reduction in peridotite and gabbro exposed by detachment faulting at the Mid-Atlantic Ridge, 15° 20′ N (ODP Leg 209): a sulfur and oxygen isotope study. Geochem Geophys Geosyst 8(8):Q08002

Baker ET (2009) Relationships between hydrothermal activity and axial magma chamber distribution, depth, and melt content. Geochem Geophys Geosyst 10(6):329–332

Baker ET, Chen YJ, Morgan JP (1996) The relationship between near-axis hydrothermal cooling and the spreading rate of mid-ocean ridges. Earth Planet Sci Lett 142(1):137–145

Baker ET, Edmonds HN, Michael PJ, Wolfgang B, Dick HJB, Snow JE, Walker SL, Banerjee NR, Langmuir CH (2004) Hydrothermal venting in magma deserts: the ultraslow-spreading Gakkel and Southwest Indian Ridges. Geochem Geophys Geosyst 5(8):217–228

Barrie CT, Hannington MD, Bleeker WI (1999) The giant Kidd Creek volcanic-associated massive sulfide deposit, Abitibi Subprovince, Canada. Econ Geol 8:247–269

Beaulieu SE, Baker ET, German CR, Maffei A (2013) An authoritative global database for active submarine hydrothermal vent fields. Geochem Geophys Geosyst 14(11):4892–4905

Bischoff JL, Seyfried WE Jr (1978) Hydrothermal chemistry of sea water from 25° to 350°C. Am J Sci 278:838–860

Bogdanov YA, Bortnikov NS, Vikent'ev IV, Gurvich EG, Sagalevich AM (1997) A new type of modern mineral-forming system: black smokers of the hydrothermal field at 14° 45′ N latitude, Mid-Atlantic Ridge. Geol Depos 39(1):58–78

Bühn B, Santos RV, Dardenne MA, de Oliveira CG (2012) Mass-dependent and mass-independent sulfur isotope fractionation ($\delta^{34}S$ and $\delta^{33}S$) from Brazilian Archean and Proterozoic sulfide deposits by laser ablation multi-collector ICP-MS. Chem Geol 312-313:163–176

Butler IB, Fallick AE, Nesbitt RW (1998) Mineralogy, sulphur isotope geochemistry and the development of sulphide structures at the Broken Spur hydrothermal vent site, 29° 10′ N, Mid-Atlantic Ridge. J Geol Soc London 155:773–785

Canfield DE (2002) Biogeochemistry of sulfur isotopes, in Stable Isotope Geochemistry, Rev. Mineral., vol. 43, edited by J. W. Valley and D. R. Cole, Mineral. Soc. of Am., Washington, D. C: 607–633

Canfield DE, Teske A (1996) Late Proterozoic rise in atmospheric oxygen concentration inferred from phylogenetic and sulfur-isotope studies. Nature 382:127–132

Cannat M, Rommevaux-Jestin C, Sauter D, Deplus C, Mendel V (1999) Formation of the axial relief at the very slow spreading Southwest Indian Ridge (49° to 69°E). J Geophys Res 104(B10):22,825−22,843

Cannat M, Rommevaux-Jestin C, Fujimoto H (2003) Melt supply variations to a magma-poor ultra-slow spreading ridge (Southwest Indian Ridge 61° to 69°E). Geochem Geophys Geosyst 4(8):9104

Cannat M, Sauter D, Mendel V, Ruellan E, Okino K, Escartin J, Combier V, Baala M (2006) Modes of seafloor generation at a melt-poor ultraslow-spreading ridge. Geology 34(7):605–608

Cannat M, Sauter D, Bezos A, Meyzen C, Humler E, Le Rigoleur M (2008) Spreading rate, spreading obliquity, and melt supply at the ultraslow spreading Southwest Indian Ridge. Geochem Geophys Geosyst 9:Q04002. https://doi.org/10.1029/2007GC001676

Cao H, Sun ZL, Liu CL, Jiang XJ, He YJ, Huang W, Shang LN, Wang LB, Zhang XL, Geng W, Shi MJ, Li DY (2018) The metallogenic mechanism and enlightenment of hydrothermal sulfide from the ultramafic-hosted hydrothermal systems at ultra-slow spreading ridge. HaiyangXuebao 40(4):61–75. https://doi.org/10.3969/j.issn.0253-4193.2018.04.006 (in Chinese with English abstract)

Charlou JL, Donval JP, Fouquet Y, Jean-Baptiste P, Holm N (2002) Geochemistry of high H_2 and CH_4 vent fluids issuing from ultramafic rocks at the Rainbow hydrothermal field (36° 14′ N, MAR). Chem Geol 191(4):345–359

Chen J, Tao CH, Liang J, Liao SL, Dong CW, Li HM, Li W, Wang Y, Yue XH, He YH (2018) Newly discovered hydrothermal fields along the ultraslow-spreading Southwest Indian Ridge around 63E°. Acta Oceanol Sin 11:61–67

Cherkashev G, Ivanov VN, Bel'tenev VI, Lazareva LI, Rozhdestvenskaya II, Samovarov ML, Poroshina I, Sergeyev MB, Stepanova TV, Dobretsova I (2010) Seafloor massive sulfides from the Equatorial Mid-Atlantic Ridge: new discoveries and perspectives. Mar Georesour Geotechnol 28(3):222–239. https://doi.org/10.1080/1064119X.2010.483308

Cherkashev G, Ivanov VN, Bel'tenev VI, Lazareva LI, Rozhdestvenskaya II, Samovarov ML, Poroshina I, Sergeyev MB, Stepanova TV, Dobretsova I, Kuznetsov VY (2013) Massive sulfide ores of the northern equatorial Mid-Atlantic Ridge. Mar Geol 53(5):607–619

Chiba H, Uchiyama N, Teagle DAH (1998) Stable isotope study of anhydrite and sulfide minerals at the TAG hydrothermal mound, Mid-Atlantic Ridge, 26°N. College station (Ocean Drilling Program):85–90

Craddock PR, Rouxel OJ, Ball LA, Bach W (2008) Sulfur isotope measurement of sulfate and sulfide by high-resolution MC-ICP-MS. Chem Geol 253:102–113

Detmers J, Brüchert V, Habicht KS, Kuever J (2001) Diversity of sulfur isotope fractionations by sulfate-reducing prokaryotes. Appl Environ Microbiol 67:888–894

Dias ÁS, Barriga F (2006) Mineralogy and geochemistry of hydrothermal sediments from the serpentinite-hosted Saldanha hydrothermal field (36° 34′ N; 33° 26′ W) at MAR, Mar. Geol. 225(1–4):157–175. https://doi.org/10.1016/j.margeo.2005.07.013

Dick HJB, Lin J, Schouten H (2003) An ultraslow-spreading class of ocean ridge. Nature 426:405–412

Douville E, Charlou JL, Oelkers EH, Bienvenu P, Colon CFJ, Donval JP, Fouquet Y, Prieur D, Appriou P (2002) The rainbow vent fluids (36° 14′ N, MAR): the influence of ultramafic rocks and phase separation on trace metal content in Mid-Atlantic Ridge hydrothermal fluids. Chem Geol 184(1–2):37–48

Duckworth RC, Knott R, Fallick AE, Rickard D, Murton BJ, van Dover C (1995) Mineralogy and Sulphur isotope geochemistry of the Broken Spur sulphides, 29° N. Mid-Atlantic Ridge 87:175–189

Engel CG, Fisher RL (1975) Granitic to ultramafic rock complexes of the Indian Ocean ridge system, western Indian Ocean. Geol Soc Am Bull 86:1553–1578

Escartin J, Smith DK, Cann J, Schouten H, Langmuir CH, Escrig S (2008) Central role of detachment faults in accretion of slow-spreading oceanic lithosphere. Nature 455(7214):790–794

Fleet ME (1970) Structural aspects of the marcasite-pyrite transformation. Can Mineral 10(2):225–231

Fornari DJ, Haymon RM, Perfit MR, Gregg TKP, Edwards MH (1998) Axial summit trough of the East Pacific Rice 9°-10°N: geological characteristics and evolution of the axial zone on fast spreading mid-ocean ridge. J Geophys Res Solid Earth 103(B5):9827–9855

Fouquet Y, Charlou JL, Barriga F (2002) Modern seafloor hydrothermal deposits hosted in ultramafic rocks. Geol. Soc. Am. Abstracts with Programs, 34(6)A: Paper No. 194–7

Fouquet Y, Cambon P, Etoubleau J, Charlou JL, Ondréas H, Barriga FJ, Cherkashev G, Semkova T, Poroshina I, Bohn M (2010) Geodiversity of hydrothermal processes along the mid-Atlantic ridge and ultramafic-hosted mineralization: a new type of oceanic Cu-Zn-Co-Au volcanogenic massive sulfide deposit. Divers Hydrothermal Syst Slow Spreading Ocean Ridges 188:321–367

Fu J, Hu Z, Zhang W, Yang L, Liu Y, Li M, Zong K, Gao S, Hu S (2016) In situ sulfur isotopes ($\delta^{34}S$ and $\delta^{33}S$) analyses in sulfides and elemental sulfur using high sensitivity cones combined with the addition of nitrogen by laser ablation MC-ICPMS. Anal Chim Acta 911: 14–26

German CR and Lin J (2004) The thermal structure of the oceanic crust, ridge-spreading and hydrothermal circulation: how well do we understand their inter-connections? in Mid-ocean ridges: hydrothermal interactions between the lithosphere and oceans, Geophys. Monogr. Ser., vol. 148, edited by C. R. German, J. Lin, and L. M. Parson, pp. 1–18, AGU, Washington, D.C.

German CR, Parson LM (1998) Distributions of hydrothermal activity along the Mid-Atlantic Ridge: interplay of magmatic and tectonic controls. Earth Planet Sci Lett 160(3):327–341

German CR, Klinkhammer GP, Rudnicki MD (1996) The Rainbow hydrothermal plume, 36° 15′ N, MAR. Geophys Res Lett 23(21): 2979–2982

German CR, Petersen S, Hannington MD (2016) Hydrothermal exploration of mid-ocean ridges: where might the largest sulfide deposits be forming? Chem Geol 420:114–126

Goldhaber MB, Kaplan IR (1975) Controls and consequences of sulfate reduction rates in recent marine sediments. Soil Sci 119:42–55

Gow PA, Wall VJ, Oliver NHS, Valenta RK (1994) Proterozoic iron oxide (Cu–U–Au–REE) deposits: further evidence of hydrothermal origin. Geology 22:633–636

Hannington MD, Scott SD (1988) Mineralogy and geochemistry of a hydrothermal silica-sulfide-sulfate spire in the caldera of Axial-Seamount, Juan de Fuca ridge. Can Mineral 26:603–625

Hannington MD, de Ronde CD, Peterse S (2005) Sea-floor tectonics and submarine hydrothermal systems. In: Hedenquist JW, Thompson JFH, Goldfarb RJ, Richards JP (eds) Economic Geology 100th Anniversary Volume. Society of Economic Geologists, Littelton, pp 111–141

Hannington MD, Jamieson J, Monecke T, Petersen S (2010) Modern sea-floor massive sulfides and base metal resources: toward an estimate of global sea-floor massive sulfide potential. Soc Econ Geol Spec Publ 15:317–338

Herzig PM, Hannington MD, Arribas A (1998) Sulfur isotopic composition of hydrothermal precipitates from the Lau back-arc: implications for magmatic contributions to seafloor hydrothermal systems. Mineral Deposita 33:226–237

Horner-Johnson BC, Gordon RG, Cowles SM, Argus DF (2005) The angular velocity of Nubia relative to Somalia and the location of the Nubia-Somalia-Antarctica triple junction. Geophys J Int 162(1):221–238

Ildefonse B, Blackman DK, John BE, Ohara Y, Miller DJ, Macleod CJ (2007) Oceanic core complexes and crustal accretion at slow-spreading ridges. Geology 35(7):623–626

Ishihara S, Sasaki A (1989) Sulfur isotopic ratios of the magnetite-series and ilmenite-series granitoids of the Sierra Nevada batholith-a reconnaissance study. Geology 17:788–791

Janecky DR, Shanks WC III (1988) Computational modeling of chemical and sulfur isotopic reaction processes in seafloor hydrothermal systems: chimneys, massive sulfides, and subjacent alteration zones. Can Mineral 26:805–825

Kase K, Yamamoto M, Shibata T (1990) Copper-rich sulfide deposits near 23° N, Mid-Atlantic Ridge: chemical composition, mineral chemistry, and sulfur isotopes: Proceedings of the Ocean Drilling Program. Sci Res 106(109):163–172

Kelley DS, Karson JA, Blackman D, Fruh-Green GL, Butterfied D, Lilley MD, Olson EJ, Schrenk MO, Roe KK, Lebon GT (2001) An off-axis hydrothermal vent field near the Mid-Atlantic Ridge at 30° N. Nature 412:145–149. https://doi.org/10.1038/35084000

Knott R, Fallick AE, Rickard D, Bäcker H (1995) Mineralogy and sulphur isotope characteristics of a massive sulphide boulder, Galapagos Rift, 85°55′ W: Geological Society of London special Publication 87: 207–222

Knott R, Fouquet Y, Honnorez J, Petersen S, Bohn M (1998) Petrology of hydrothermal mineralization: a vertical section through the TAG mound. Proc Ocean Drill Program Sci Results 158:5–26

Lalou C, Münch U, Halbach P, Reyss JL (1998) Radiochronological investigation of hydrothermal deposits from the MESO zone, Central Indian Ridge. Mar Geol 149(1–4):243–254

Lein AY, Ulyanova NV, Ulyanov AA, Cherkashev GA, Stepanova TV (2001) Mineralogy and geochemistry of sulfide ores in ocean-floor hydrothermal fields associated with serpentinite protrusions. Russ J Earth Sci 3(5):371–393

Li JB, Jian HC, Chen YS, Singh SC, Ruan AG, Qiu XL, Zhao MH, Wang XG, Niu XG, Ni JY, Zhang JZ (2015) Seismic observation of an extremely magmatic accretion at the ultraslow spreading Southwest Indian Ridge. Geophys Res Lett 42(8):2656–2663

Liao SL, Tao CH, Li HM, Barriga FJAS, Liang J, Yang WF, Yu JY, Zhu GW (2018) Bulk geochemistry, sulfur isotope characteristics of the Yuhuang-1 hydrothermal field on the ultraslow-spreading Southwest Indian Ridge. Ore Geol Rev 96:13–27

Lowell RP, Rona PA (2002) Seafloor hydrothermal systems driven by the serpentinization of peridotite. Geophys Res Lett 29(11(26)):1–4

Lowell RP, Yao YF (2002) Anhydrite precipitation and the extent of hydrothermal recharge zones at ocean ridge crests. J Geophys Res 107(B9):2183–EPM 2-9. https://doi.org/10.1029/2001JB001289

Lowell RP, Yao YF, Germanovich LN (2003) Germanovich, anhydrite precipitation and the relationship between focused and diffuse flow in seafloor hydrothermal systems. J Geophys Res 108(B9):2424. https://doi.org/10.1029/2002JB002371

Lusk J, Bray DM (2002) Phase relations and the electrochemical determination of sulfur fugacity for selected reactions in the Cu–Fe–S and Fe–S systems at 1 bar and temperatures between 185 and 460 °C. Chem Geol 192(3–4):227–248

Marques AFA, Barriga FJAS, Scott SD (2007) Sulfide mineralization in an ultramafic-rock hosted seafloor hydrothermal system: from serpentinization to the formation of Cu-Zn-(Co)-rich massive sulfides. Mar Geol 245(1–4):20–39

Mason PRD, Kosler J, de Hoog JCM, Sylvester PJ, Meffan-Main S (2006) In situ determination of sulfur isotopes in sulfur-rich materials by laser ablation multiple-collector inductively coupled plasma mass spectrometry (LA-MC-ICP-MS). J Anal At Spectrom 21:177–186

McCaig AM, Cliff RA, Escartin J, Fallick AE, Macleod CJ (2007) Oceanic detachment faults focus very large volumes of black smoker fluids. Geology 35(10):935–938

Melchert B, Devey Colin W, German CR, Lackschewitz K, Seifert R, Walter M, Mertens C, Yoerger DR, Baker ET, Paulick H, Nakamura K (2008) First evidence for high-temperature off-axis venting of deep crustal/mantle heat: the Nibelungen hydrothermal field, southern Mid-Atlantic Ridge. Earth Planet Sci Lett 275:61–69. https://doi.org/10.1016/j.epsl.2008.08.010

Minshull TA, Muller MR, White RS (2006) Crustal structure of the Southwest Indian Ridge at 66° E: seismic constraints. Geophys J Int 166(1):135–147

Mozgova NN, Borodaev YS, Gablina IF, Cherkashev GA, Stepanova TV (2005) Mineral assemblages as indicators of the maturity of oceanic hydrothermal sulfide mounds. Lithol Miner Resour 40(4):293–319

Münch U, Lalou C, Halbach P, Fujimoto H (2001) Relict hydrothermal events along the super-slow Southwest Indian spreading ridge near 63° 56′ E-mineralogy, chemistry and chronology of sulfide samples. Chem Geol 177(3–4):341–349

Nayak B, Halbach P, Pracejus B, Münch U (2014) Massive sulfides of Mount Jourdanne along the super-slow spreading Southwest Indian Ridge and their genesis. Ore Geol Rev 63:115–128

O'Hanley DS (1992) Solution to the volume problem in serpentinization. Geology 20(8):705–708

Ohmoto H, Goldhaber MB (1997) Sulfur and carbon isotopes. In: Barnes HL (ed) Geochemistry of hydrothermal ore deposits. Wiley, pp 517–611

Ohmoto H, Rye RO (1979) Isotopes of sulfur and carbon. In: Barnes HL (ed) Geochemistry of hydrothermal ore deposits, 2nd edn. Wiley, New York, pp 509–567

Ohmoto H, Mizukami M, Drummond SE, Eldridge CS, Pisutha-Arnond V, Lenagh TC (1983) Chemical processes of Kuroko formation. Econ Geol Monogr 5:570–604

Ono S, Shanks WC III, Rouxel OJ, Rumble D (2007) S-33 constrains on the seawater sulfate contribution in modern seafloor hydrothermal vent sulfides. Geochim Cosmochim Acta 71(5):1170–1182

Peter JM, Shanks WC III (1992) Sulfur, carbon, and oxygen isotope variations in submarine hydrothermal deposits of Guaymas basin, Gulf of California, USA. Geochim Cosmochim Acta 56:2025–2040

Peters JM, Strauss H, Farquhar J, Ockert C, Eickmann B, Jost CL (2010) Sulfur cycling at the Mid-Atlantic Ridge: a multiple sulfur isotope approach. Chem Geol 269:180–196

Ranero CR, Reston TJ (1999) Detachment faulting at ocean core complexes. Geology 27(11):983–986

Rees CE, Jenkins WJ, Monster J (1978) The sulphur isotope geochemistry of ocean water sulphate. Geochim Cosmochim Acta 42:377–382

Rouxel O, Fouquet Y, Ludden JN (2004) Copper isotope systematics of the Lucky Strike, Rainbow and Logatchev seafloor hydrothermal fields on the Mid Atlantic Ridge. Econ Geol 99:585–600

Rouxel O, Shanks WC III, Bach W, Edwards K (2008) Intergrated Fe- and S-isotope study of seafloor hydrothermal vents at East Pacific rise 9-10° N. Chem Geol 252(3–4):214–227

Sakai H, Des Marais DJ, Ueda A, Moore JG (1984) Concentrations and isotope ratios of carbon, nitrogen, and sulfur in ocean-floor basalts. Geochim Cosmochim Acta 48:2433–2442

Santosh M, Masuda H (1991) Reconnaissance oxygen and sulfur isotopic mapping of Pan-African alkali granites and syenites in the southern Indian Shield. Geochem J 25:173–185

Sauter D, Patriat P, Rommevaux-Jestin C, Cannat M, Briais A, Gallieni Shipboard Scientific Party (2001) The Southwest Indian Ridge between 49° 15′ E and 57° E: focused accretion and magma redistribution. Earth Planet Sci Lett 192(3):303–317

Sauter D, Carton H, Mendel V, Munschy M, Rommevaux-Jestin C, Schott JJ, Whitechurch H (2004) Ridge segmentation and the magnetic structure of the Southwest Indian Ridge (at 50° 30′ E, 55° 30′ E and 66° 20′ E): implications for magmatic processes at ultraslow-spreading centers. Geochem Geophys Geosyst 5:Q05K08. https://doi.org/10.1029/2003GC000581

Sauter D, Cannat M, Meyzen C, Bezos A, Patriat P, Humler E, Debayle E (2009) Propagation of a melting anomaly along the ultraslow Southwest Indian Ridge between 46° E and 52° 20′ E: interaction with the Crozet hotspot? Geophys J Int 179(2):687–699

Sauter D, Cannat M, Rouméjon S, Andreani M, Briot D, Bronner A, Brunelli D, Carlut J, Delacour A, Guyader V, Macleod CJ, Manatschal G, Mendel V, Ménez B, Pasini V, Ruellan E, Searle R (2013) Continuous exhumation of mantle-derived rocks at the Southwest Indian Ridge for 11 million years. Nat Geosci 6(4):314–320

Schmidt K, Koschinsky A, Garbe-Schönberg D, de Carvalho LM, Seifert R (2007) Geochemistry of hydrothermal fluids from the ultramafic-hosted Logatchev hydrothermal field, 15° N on the Mid-Atlantic Ridge: temporal and spatial investigation. Chem Geol 242(1):1–21

Schwarzenbach E, Früh-Green GL, Bernasconi SM, Alt JC, Shanks WC III, Gaggero L, Crispini L (2012) Sulfur geochemistry of peridotite-hosted hydrothermal systems: comparing the Ligurian ophiolites with oceanic serpentinites. Geochim Cosmochim Acta 91:283–305

Seal RR (2006) Sulfur isotope geochemistry of sulfide minerals. Rev Mineral Geochem 61:633–677

Seyfried WE Jr, Bischoff JL (1981) Experimental seawater-basalt interaction at 300°C, 500 bars, chemical exchange, secondary mineral formation and implication for the transport of heavy metals. Geochim Cosmochim Acta 45:135–147

Shanks WC III (2001) Stable isotopes in seafloor hydrothermal systems. Rev Mineral Geochem 43:469–525

Shanks WC III, Seyfried WE Jr (1987) Stable isotope studies of vent fluids and chimney minerals, southern Juan de Fuca Ridge: sodium metasomatism and seawater sulfate reduction. J Geophys Res 92:11387–11399

Shanks WC III, Bohlke JK, Seal RR (1995) Stable isotopes in mid-ocean ridge hydrothermal systems: interactions between fluids, minerals, and organisms. In: Humphris SE, Zierenberg RA, Mullineaux LS, Thomson RE (eds) Seafloor hydrothermal systems: physical, chemical, biological, and geological interactions, vol 91. Geophys Monogr, pp 194–221

Shibata T, Thompson G, Frey FA (1979) Tholeiitic and alkali basalts from the Mid-Atlantic Ridge at 43°N. Contrib Mineral Petrol 70:127–141

Sleep NII (1991) Hydrotherma circulation, anhydrite precipitation, and thermal structure at ridge axes. J Geophys Res 96:2375–2387

Standish JJ, Sims KWW (2010) Young off-axis volcanism along the ultraslow spreading Southwest Indian Ridge. Nat Geosci 3:286–292

Tao CH, Lin J, Guo SQ, Chen YS, Wu GH, Han XQ, German CR, Yoerger DR, Zhou N, Li HM, Su X, Zhu J (2012) First active hydrothermal vents on an ultraslow-spreading center: Southwest Indian Ridge. Geology 40(1):47–50

Tao CH, Li HM, Jin XB, Zhou JP, Wu T, He YH, Deng XM, Gu CH, Zhang GY, Liu WY (2014) Seafloor hydrothermal activity and polymetallic sulfide exploration on the southwest Indian ridge. Chin Sci Bull 59(19):2266–2276

Tao CH, Seyfried WE Jr, Lowell RP, Liu YL, Liang J, Guo ZK, Ding K, Zhang HT, Liu J, Qiu L, Egorv I, Liao SL, Zhao MH, Zhou JP, Deng XM, Li HM, Wang HC, Cai W, Zhang GY, Zhou HW, Lin J, Li W (2020) Deep high-temperature hydrothermal circulation in a detachment faulting system on the ultra-slow spreading ridge. Nat Commun. https://doi.org/10.1038/s41467-020-15062-w

Wang YJ (2012) Comparision study of mineralization of Kairei and Edmond active hydrothermal fields in central Indian ridge. Doctoral disseration. 129 pp. Zhejiang University, China. (in Chinese with English abstract)

Wetzel LR, Shock EL (2000) Distinguishing ultramafic-from basalt-hosted submarine hydrothermal systems by comparing calculated vent fluid compositions. J Geophys Res Solid Earth 105(B4):8319–8340

Woodruff LG, Shanks WC III (1988) Sulfur isotope study of chimney minerals and vent fluids from 21° N, East Pacific Rise: hydrothermal sulfur sources and disequilibrium sulfate reduction. J Geophys Res 93(B5):4562–4572

Wortmann UG, Bernasconi SM, Böttcher ME (2001) Hypersulfidic deep biosphere indicates extreme sulfur isotope fractionation during single-step microbial sulfate reduction. Geology 29:647–650

Yang AY, Zhao TP, Zhou MF, Deng XG (2017a) Isotopically enriched N-MORB: a new geochemical signature of off-axis plume-ridge interaction-a case study at 50° 28′ E, Southwest Indian Ridge. J Geophys Res Solid Earth 122:191–213

Yang WF, Tao CH, Li HM, Liang J, Liao SL, Long JP, Ma ZB, Wang LS (2017b) $^{230}Th/^{238}U$ dating of hydrothermal sulfides from Duanqiao hydrothermal field, Southwest Indian Ridge. Mar Geophys Res 38: 1–13

Ye J (2010) Mineralization of polymetallic sulfides on ultraslow spreading Southwest Indian Ridge at 49.6° E. Doctoral disseration. 129 pp. Graduate University of Chinese Academy of Sciences, China. (in Chinese with English abstract)

Yuan B, Yu HJ, Yang YM, Zhao YX, Yang JC, Xu Y, Lin Z (2018) Zone refinement related to the mineralization process as evidenced by mineralogy and element geochemistry in a chimney fragment from the Southwest Indian Ridge at 49.6° E. Chem Geol 482:46–60

Zeng ZG, Ma Y, Chen S, Selby D, Wang XY, Yin XB (2016) Sulfur and lead isotopic compositions of massive sulfides from deep-sea hydrothermal systems: implications for ore genesis and fluid circulation. Ore Geol Rev 87:155–171

Zhou HY, Dick HJB (2013) Thin crust as evidence for depleted mantle supporting the Marion Rise. Nature 494(7436):195–200. https://doi.org/10.1038/nature11842

Zhu ZY, Cook NJ, Yang T, Ciobanu CL, Zhao KD, Jiang SY (2016) Mapping of sulfur isotopes and trace elements in sulfides by LA-(MC)-ICP-MS: potential analytical problems, improvements and implications. Fortschr Mineral 6:110

Zierenberg RA (1994) Sulfur content of sediments and sulfur isotope values of sulfide and sulfate minerals from Middle Valley: Proceedings of the Ocean Drilling Program. Sci Res 139:739–748

Zierenberg RA, Shanks WC III (1988) Isotopic studies of epigenetic features in metalliferous sediment, Atlantis II Deep, Red Sea. Can Mineral 26:737–753